START 0000021

WATER RESOURCES RESEARCH, VOL. 21, NO. 3, PAGES 346–358, MARCH 1985

NOTICE: This material may be protected by copyright law (Title 17 U.S. Code)

Finite Element Matrix and Mass Balance Computational Schemes for Transport in Variably Saturated Porous Media

PETER S. HUYAKORN, JAMES W. MERCER, AND DAVID S. WARD

GeoTrans, Inc., Herndon, Virginia

An upstream-weighted residual finite element formulation is developed for the numerical simulation of solute transport in variably saturated porous media. Included in this formulation is an influence coefficient scheme for element matrix evaluation and a mass balance computation scheme. These schemes are not only simple to implement but also cost effective. Three examples are provided to verify the numerical techniques and demonstrate the utility of the computer model. These examples indicate that mass balance information serves a useful purpose as a screening device for examining the numerical solution. They also show certain behavior of the mass balance error as well as numerical difficulties associated with the manner in which the finite element formulation of the transport equation is performed. Finally, information on the CPU time and cost required to solve the three example problems is provided to show the cost effectiveness of the present transport model. Although the present analysis considers only two dimensions, the schemes described can be extended to three dimensions, where the time and cost savings are more significant.

INTRODUCTION

The majority of hazardous and low-level radioactive wastes that are placed in the subsurface are affected by the physical and chemical processes active in the variably saturated zone [*Mercer et al.*, 1983]. In addition, accidental spills and land application of materials such as pesticides are affected by the variably saturated zone. As a means to help better assess and control contamination problems, computer models have been developed to simulate flow and transport in the variably saturated zone (see, for example, a review by *Oster* [1982]).

Many of these models are based on analytical or semi-analytical solutions and are limited to simple one-dimensional problems. Typical examples of the analytical models are presented by *Warrick et al.* [1971], *Smiles et al.* [1978], *van Genuchten and Alves* [1982], and *Watson and Jones* [1982]. Recognizing the limitations of the analytical approach, several researchers resorted to numerical methods. Most of the earlier numerical models are based on the finite difference approach (see, for example, *Bresler and Hanks* [1969], *Bresler* [1973], and *Kirda et al.* [1973]). Recently, there has been a tendency to use the finite element solution approach. Models based on such an approach have been developed by *Duguid and Reeves* [1976], *Segol* [1977], *van Genuchten et al.* [1977], *Pickens and Gillham* [1980], and *Yeh and Ward* [1981]. Surprisingly, all but one of these models lack a scheme for checking whether the numerical solution obtained satisfies the integral mass balance equation for the entire flow region. Only the model presented by *Yeh* [1981] has a reliable mass balance computational scheme. However, the particular scheme, which was implemented in the code documented by *Yeh and Ward* [1981], requires rather excessive computational effort.

This paper is the second in our series of papers that deal with the development and application of multidimensional finite element models. The first paper [*Huyakorn et al.*, 1984] dealt with variably saturated flow in two dimensions, whereas this paper discusses solute transport in two dimensions. The prime motivation in presenting this work is to provide innovative techniques for enhancing the computational efficiency and accuracy of the finite element approach, thus making it more attractive to use in solving complex field problems. The importance of these techniques will be realized in a subsequent paper that deals with flow and transport in three dimensions.

In this paper, we refer to the variably saturated flow aspects discussed by *Huyakorn et al.* [1984] but focus on solute transport simulations. The processes considered include hydrodynamic dispersion, advection, adsorption, and chemical degradation or radioactive decay. After the basic equations for transport in variably saturated porous media have been discussed, an upstream-weighted residual finite element formulation designed to alleviate the problem of numerical oscillations is presented. Included as part of this formulation is an influence coefficient scheme that enables element matrices to be evaluated in a simple and efficient manner by avoiding costly numerical integration. In addition, a newly developed mass balance computational algorithm is presented as a screening device for checking the numerical solution obtained. Finally, the numerical model is tested using a set of one- and two-dimensional examples designed to demonstrate the utility and advantages of the techniques described.

Although the present paper focuses on two-dimensional transport problems, the formulation can be readily extended to three dimensions. Particularly, influence coefficient formulas can be developed for simple three-dimensional elements such as rectangular and triangular prisms. Furthermore, as will be shown in the forthcoming paper, the influence coefficient technique is adaptable to a slice successive overrelaxation matrix scheme (SSOR) which allows a complex problem with several thousand nodal unknowns to be solved efficiently.

GOVERNING EQUATIONS

The advective-dispersive transport of a nonconservative constituent in a porous medium partially saturated with water may be represented by the following equation [see *Bear*, 1979]:

$$\frac{\partial}{\partial x_i}\left(\phi S_w \tilde{D}_{ij}\frac{\partial c}{\partial x_j}\right) - \frac{\partial}{\partial x_i}(V_i c) = \frac{\partial}{\partial t}[\phi S_w c + \rho_s(1-\phi)c_s] - qc^* + \lambda[\phi S_w c + \rho_s(1-\phi)c_s] \quad (1)$$

Copyright 1985 by the American Geophysical Union.

Paper number 4W1451.
0043-1397/85/004W-1451$05.00

where the usual summation convention is used with subscripts i and j ranging from 1 to 2 for the two-dimensional situation, $\bar{D}_{ij}$ is the hydrodynamic dispersion tensor, c is the concentration of the dissolved constituent, V_i is the Darcy velocity, S_w is the water saturation, ρ_s is the density of the solid material, ϕ is the porosity, c_s is the concentration of the adsorbed constituent in the solid phase, q is the volumetric flow rate of fluid injection (or withdrawal) per unit volume of the porous medium, c^* is the concentration of the constituent in the injected fluid, and λ is the decay constant.

In (1) it is implicitly assumed that the fluid compressibility is negligible. Furthermore, the hydrodynamic dispersion tensor may be expressed as

$$\phi S_w \bar{D}_{ij} = \alpha_T |V| \delta_{ij} + (\alpha_L - \alpha_T) \frac{V_i V_j}{|V|} + \phi S_w \tau D^* \delta_{ij} \qquad (2)$$

where α_L and α_T are the longitudinal and the transverse dispersities, respectively, δ_{ij} is the Kronecker delta, $|V|$ is the absolute value of the Darcy velocity, τ is the tortuosity, and D^* is the coefficient of molecular diffusion.

It is also assumed that a linear equilibrium isotherm can be used to relate the adsorbed concentration c_s and the solution concentration c. This enables us to write (1) in the form

$$\frac{\partial}{\partial x_i}\left(D_{ij}\frac{\partial c}{\partial x_j}\right) - \frac{\partial}{\partial x_i}(V_i c) = \frac{\partial}{\partial t}(\phi S_w \kappa c) + \lambda \phi S_w \kappa c - qc^* \qquad (3)$$

where

$$D_{ij} = \phi S_w \bar{D}_{ij} \qquad (4a)$$

$$\kappa = 1 + \frac{\rho_s(1-\phi)k_d}{\phi S_w} = 1 + \frac{\rho_B k_d}{\phi S_w} \qquad (4b)$$

in which k_d is the distribution coefficient and ρ_B is the bulk density defined as $\rho_B = (1-\phi)\rho_s$. Note that the effective retardation coefficient κ is a function of water saturation S_w. The value of $\kappa - 1$ varies inversely as S_w. Equation (3) is a primitive form of the transport equation. It can be converted to another form that is more convenient for finite element discretization. This is accomplished by expanding the advective and the mass accumulation terms and using the continuity equation for water flow,

$$-\frac{\partial V_i}{\partial x_i} = \frac{\partial}{\partial t}(\phi S_w) - q \qquad (5)$$

Performing the necessary steps, one obtains

$$\frac{\partial}{\partial x_i}\left(D_{ij}\frac{\partial c}{\partial x_j}\right) - V_i\frac{\partial c}{\partial x_i} + c\frac{\partial}{\partial t}(\phi S_w) - qc$$

$$= \phi S_w \kappa \frac{\partial c}{\partial t} + c\frac{\partial}{\partial t}(\phi S_w) + c\frac{\partial}{\partial t}(\rho_B k_d) - qc^* + \lambda \phi S_w \kappa c \qquad (6)$$

Assuming that the term containing time derivative of $\rho_B k_d$ is negligible, equation (6) may be reduced to

$$\frac{\partial}{\partial x_i}\left(D_{ij}\frac{\partial c}{\partial x_j}\right) - V_i\frac{\partial c}{\partial x_i} = \phi S_w \kappa\left(\frac{\partial c}{\partial t} + \lambda c\right) + q(c - c^*) \qquad (7)$$

Equation (7) is the required form of the solute transport equation. The initial and boundary conditions associated with it may be represented by

$$c(x_i, 0) = c_0 \qquad (8)$$

$$c(x_i, t) = \bar{c} \qquad \text{on } B_1 \qquad (9)$$

$$D_{ij}\frac{\partial c}{\partial x_j} n_i = q_c{}^D \qquad \text{on } B_2 \qquad (10)$$

$$D_{ij}\frac{\partial c}{\partial x_j} n_i - V_i n_i c = q_c{}^T \qquad \text{on } B_3 \qquad (11)$$

where B_1 is the boundary portion where concentration is prescribed as $\bar{c}$, n_i is the outward unit normal vector on the boundary, B_2 and B_3 are the boundary portions where the dispersive and the total solute mass fluxes are prescribed as $q_c{}^D$ and $q_c{}^T$, respectively, and the sign convention for the boundary fluxes is positive for mass injection and negative for mass withdrawal.

UPSTREAM-WEIGHTED RESIDUAL FINITE ELEMENT APPROXIMATION

To discretize the transport equation (7) using the upstream-weighted residual finite element method, the function c is represented by a trial function of the form

$$\hat{c}(x_i, t) = N_J(x_i)c_J(t) \qquad J = 1, 2, \cdots, n \qquad (12)$$

where $N_J(x_i)$ and $c_J(t)$ are the basis functions and nodal values of concentration at time t and n is the number of nodes in the finite element network.

In the upstream-weighted residual procedure presented by *Huyakorn and Nilkuha* [1979], the weighted residual integral equation is obtained using asymmetric weighting functions W_I to weight the spatial derivative terms of the transport equation and the basis functions N_I to weight the remaining terms. Application of this procedure to (7) yields

$$\int_R W_I\left[\frac{\partial}{\partial x_i}\left(D_{ij}\frac{\partial \hat{c}}{\partial x_j}\right) - V_i\frac{\partial \hat{c}}{\partial x_i}\right] dR$$

$$- \int_R N_I\left[\phi S_w \kappa\left(\frac{\partial \hat{c}}{\partial t} + \lambda \hat{c}\right) + q(\hat{c} - c^*)\right] dR = 0 \qquad (13)$$

$$I = 1, 2, \cdots, n$$

where W_I is the asymmetric weighting function for node I and the integration is performed over the solution region R.

Using Green's theorem to remove the second derivative and substituting for $\hat{c}$, one obtains

$$\int_R \left(D_{ij}\frac{\partial W_I}{\partial x_i}\frac{\partial N_J}{\partial x_j} + V_i W_I \frac{\partial N_J}{\partial x_i}\right) c_J\, dR$$

$$+ \int_R \phi S_w \kappa N_I N_J\left(\frac{dc_J}{dt} + \lambda c_J\right) dR - \int_R N_I\, q(c^* - N_J c_J)\, dR$$

$$- \int_B W_I\left(D_{ij}\frac{\partial \hat{c}}{\partial x_j}\right) n_i\, dB = 0 \qquad I = 1, 2, \cdots, n \qquad (14)$$

where B is the boundary of the solution region and n_i is the outward unit vector normal to B. Equation (14) can be expressed in the form

$$(E_{IJ} + B_{IJ}{}^*)c_J + \bar{B}_{IJ}\frac{dc_J}{dt} = \bar{F}_I \qquad I = 1, 2, \cdots, n \qquad (15)$$

where

$$E_{IJ} = \sum_e E_{IJ}{}^e$$

$$= \sum_e \int_{R^e}\left(D_{ij}\frac{\partial W_I}{\partial x_i}\frac{\partial N_J}{\partial x_j} + V_i W_I \frac{\partial N_J}{\partial x_i}\right) dR \qquad (16a)$$

$$B_{IJ}{}^* = \sum_e B_{IJ}{}^{*e} = \sum_e \int_{R^e} (\lambda \phi S_w \kappa) N_I N_J\, dR \qquad (16b)$$

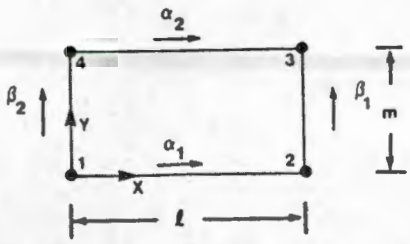

Fig. 1. Typical rectangular element showing the positive sign convention for upstream parameters α_1, α_2, β_1, and β_2.

$$\tilde{B}_{IJ} = \sum_e \tilde{B}_{IJ}^e = \sum_e \int_{R^e} (\phi S_w \kappa)\, N_I\, N_J\, dR \tag{16c}$$

$$F_I = \sum_e F_I^e = \sum_e \left[\int_{R^e} N_I\, q(c^* - N_J c_J)\, dR + \int_{B^e} W_I \left(D_{ij} \frac{\partial \hat{c}}{\partial x_j} \right) n_i\, dB \right] \tag{16d}$$

where R^e is the element subdomain enclosed by boundary B^e and $\sum_e$ is the summation over the total number of elements.

Time integration of (14) is performed in a standard manner using a general finite difference approximation which leads to [see *Huyakorn and Pinder*, 1983]

$$\left(\omega(E_{IJ} + B_{IJ}^*) + \frac{\tilde{B}_{IJ}}{\Delta t_k} \right) c_J^{k+1} = (\omega - 1)(E_{IJ} + B_{IJ}^*) c_J^k + \frac{\tilde{B}_{IJ}}{\Delta t_k} c_J^k + \omega F_I^{k+1} + (1 - \omega) F_I^k \qquad I = 1, 2, \cdots, n \tag{17}$$

where k and $k + 1$ correspond to previous and current time levels, respectively, Δt_k is the time step, and ω is a time weighting factor.

In this work, we elect to use the unconditionally stable Crank-Nicolson time stepping scheme, which corresponds to $\omega = 0.5$ and gives a second-order temporal approximation. Recognizing that element matrices may need to be computed for each time step and the cost of such computation may be substantial, we adopt the influence coefficient technique described in the first paper of the series [*Huyakorn et al.*, 1984]. This technique is extended herein to deal with a more general case involving advective-dispersive transport and the use of upstream weighting functions.

Consider the rectangular element with the local node numbering and the notation for upstream weighting factors shown in Figure 1. Note that α_1, α_2, β_1, and β_2 are the upstream factors associated with sides 12, 43, 23, and 14, respectively. The signs of the upstream factors are considered positive in the directions depicted. Expressions of the asymmetric upstream weighting functions can be found in the work by *Huyakorn* [1977]. To evaluate the element matrix $[E]^e$ in (16*a*), we first express it in the form

$$[E]^e = [E_D]^e + [E_v]^e \tag{18}$$

where $[E_D]^e$ and $[E_v]^e$ are the portions corresponding to the dispersive and advective terms of the transport equation, respectively.

Replacing x_1 and x_2 by x and y and using the approach presented in the first paper, we obtain the following expression for $[E_D]^e$:

$$[E_D]^e = \langle D_{xx} \rangle \frac{m}{l} [E_D^{xx}]^e + \langle D_{yy} \rangle \frac{l}{m} [E_D^{yy}]^e + \langle D_{xy} \rangle [E_D^{xy}]^e \tag{19a}$$

where l and m are the length and the height of the rectangle; $\langle D_{xx} \rangle$, $\langle D_{yy} \rangle$, and $\langle D_{xy} \rangle$ are centroidal values of components D_{11}, D_{22}, and D_{12} of the hydrodynamic dispersion tensor, respectively; and $[E_D^{xx}]^e$, $[E_D^{yy}]^e$, and $[E_D^{xy}]^e$ are influence coefficient matrices given in Appendix 1.

As can be seen, (19*a*) enables $[E_D]^e$ to be evaluated in a simple manner. Similarly, the advective element matrix $[E_v]^e$ can be evaluated using the following formula:

$$[E_v]^e = \langle V_x \rangle \frac{m}{2} ([E_v^x]^e + [E_v^x]_u^e) + \langle V_y \rangle \frac{l}{2} ([E_v^y]^e + [E_v^y]_u^e) \tag{19b}$$

where $\langle V_x \rangle$ and $\langle V_y \rangle$ are centroidal values of V_x and V_y, respectively; and $[E_v^x]^e$, $[E_v^y]^e$, $[E_v^x]_u^e$, and $[E_v^y]_u^e$ are influence coefficient matrices given in Appendix 2.

Note that $[E_v^x]_u$ and $[E_v^y]_u$ are directly dependent on the upstream weighting factors. These matrices vanish when α_i and β_i ($i = 1, 2$) are set to zero, in which case the upstream-weighted residual formulation reduces to the standard Galerkin formulation.

The remaining element matrices are matrices $[B^*]^e$ and $[\tilde{B}]^e$, which can also be easily evaluated as follows:

$$[B^*]^e = \frac{lm}{4} \langle \lambda \phi S_w \kappa \rangle [M]^e \tag{20}$$

and

$$[\tilde{B}]^e = \frac{lm}{4} \langle \phi S_w \kappa \rangle [M]^e \tag{21}$$

where $[M]^e$ is the influence coefficient mass matrix given in Appendix 1. Note that $[M]^e$ is nondiagonal because a lumping procedure was not used in the present finite element formulation. We avoid the lumping procedure because it generally degrades the accuracy of the finite element solution of the transport equation as demonstrated by *Gresho et al.* [1976] and *Huyakorn and Nilkuha* [1979].

In a case involving boundary fluxes and sinks or sources, the element right-hand side vector given in (16*d*) is nonzero. It can be evaluated using the procedure described in the first paper. It is apparent from Appendices 1 and 2 that the influence coefficient matrices require very little computational effort to evaluate. Thus one can expect the CPU time required by the influence coefficient technique to be just a small fraction of that required by the usual procedure for element matrix computation via numerical integration.

Although we have dealt with element matrices for rectangular elements, the given influence coefficient approach can be readily extended to deal with triangular elements. For such elements the upstream weighting functions presented by *Huyakorn* [1977] may be used to generate the influence coefficient matrices.

After the element matrix computation and element assembly, a system of algebraic equations is obtained. Boundary conditions can be applied in the usual manner by a proper modification of the global coefficient matrix and the right-hand side vector. The final system of equations can be solved efficiently using a direct solver designed to handle an asymmetric banded matrix.

MASS BALANCE COMPUTATION

In view of the fact that several numerical difficulties may be encountered in the simulation of flow and transport in variably saturated porous media, it is desirable to develop an effective scheme for assessing mass balance errors. Computation of a mass balance in a finite difference scheme is fairly straightforward and routinely performed. For the finite element method the mass balance computation is not as straightforward. The formulation of a mass balance scheme is presented in this section.

First, the mass balance over the entire solution region R is obtained by integrating the original governing (3) and applying Green's theorem to the dispersive and advective terms. This leads to the following mass balance integral equation:

$$\int_B \left(D_{ij}\frac{\partial c}{\partial x_j} - V_i c\right) n_i \, dB - \int_R \left[\frac{\partial}{\partial t}(\phi S_w \kappa c) + \phi\lambda S_w \kappa c\right] dR + \int_R qc^* \, dR = 0 \qquad (22)$$

For the sake of simplicity it is assumed that qc^* correspond to the contributions from wells located at specified nodal points. Thus

$$\int_R qc^* \, dR = \int_R \left[\sum_{l'=1}^{n_w} Q_{l'}\,\delta(\mathbf{x} - \mathbf{x}_{l'}) c_{l'}^*\right] dR = \sum_{l'=1}^{n_w} Q_{l'}\, c_{l'}^* \qquad (23)$$

where $Q_{l'}$ is the flow rate of the well located at $\mathbf{x}_{l'}$, n_w is the total number of wells, $\delta(\mathbf{x} - \mathbf{x}_{l'})$ is the Dirac delta function, and $c_{l'}^*$ is the concentration of the fluid in the well. Note that $Q_{l'}$ is considered to be positive for fluid injection and negative for fluid withdrawal. For the case of a pumping well, $c_{l'}^*$ corresponds to the concentration of the pumped fluid and thus $c_{l'}^* = c_{l'}$. For the case of an injection well, $c_{l'}^*$ is the concentration of the injected fluid. Combining (22) and (23) gives

$$\int_B \left(D_{ij}\frac{\partial c}{\partial x_j} - V_i c\right) n_i \, dB - \int_R \frac{\partial}{\partial t}(\phi S_w \kappa c)\, dR - \int_R \phi\lambda S_w \kappa c \, dR + \sum_{l'=1}^{n_w} Q_{l'} c_{l'}^* = 0 \qquad (24)$$

The second integral term of (24) may be manipulated further by expanding the time derivative and using (4*b*) to substitute for the retardation coefficient κ. Thus

$$\frac{\partial}{\partial t}(\phi S_w \kappa c) = \phi S_w \kappa \frac{\partial c}{\partial t} + c\frac{\partial}{\partial t}(\phi S_w + \rho_B k_d) \simeq \phi S_w \kappa \frac{\partial c}{\partial t} + c\frac{\partial}{\partial t}(\phi S_w) \qquad (25)$$

Combining (24) and (25) and rearranging the terms, one obtains

$$\int_B \left(D_{ij}\frac{\partial c}{\partial x_j} - V_i c\right) n_i \, dB - \int_R \left[\phi S_w \kappa\left(\frac{\partial c}{\partial t} + \lambda c\right)\right] dR - \int_R c\frac{\partial}{\partial t}(\phi S_w)\, dR + \sum_{l'=1}^{n_w} Q_{l'} c_{l'}^* = 0 \qquad (26)$$

If the exact solution of the transport problem is substituted into (26), the right-hand side will be zero. However, if an approximate finite element solution, $\hat{c} = N_J c_J$, is substituted, the right-hand side of (26) will be nonzero and will correspond to the rate of material loss $\dot{\varepsilon}_M$, that is,

$$\dot{\varepsilon}_M = \int_B \left(D_{ij}\frac{\partial \hat{c}}{\partial x_j} - V_i \hat{c}\right) n_i \, dB - \int_R \phi\kappa S_w N_J \left(\frac{dc_J}{dt} + \lambda c_J\right) dR - \int_R N_J c_J \frac{\partial}{\partial t}(\phi S_w)\, dR + \sum_{l'=1}^{n_w} Q_{l'} c_{l'}^* \qquad (27)$$

Next, we make use of the following properties of the basis functions:

$$\sum_{l_*=1}^{n_B} N_{l_*}(x, y) = 1 \qquad \forall\,(x, y) \text{ on } B \qquad (28)$$

$$\sum_{l=1}^{n} N_l(x, y) = 1 \qquad \forall\,(x, y) \text{ in } R \qquad (29)$$

where, as before, n is the total number of nodes in the solution region and n_B is the number of nodes on the boundary.

We also recall from the first paper that the term $\partial(\phi S_w)/\partial t$ in (27) corresponds the storage term in the governing equation for water flow. Assuming that the fluid compressibility is small compared to the compressibility of the porous medium, $\partial(\phi S_w)/\partial t$ may be expressed as

$$\frac{\partial}{\partial t}(\phi S_w) = \left(S_w S_s + \phi\frac{dS_w}{d\psi}\right)\frac{\partial \psi}{\partial t} = \eta\frac{\partial \psi}{\partial t} \qquad (30)$$

where S_s is the coefficient of specific storage, η is the overall coefficient of water storage capacity, and ψ is the pressure head.

Combining (27)–(30), one obtains

$$\dot{\varepsilon}_M = \sum_{l_*=1}^{n_B} \int_B N_{l_*}\left(D_{ij}\frac{\partial \hat{c}}{\partial x_j} - V_i \hat{c}\right) n_i \, dB - \sum_{l=1}^{n} \int_R \phi S_w \kappa N_l N_J \left(\frac{dc_J}{dt} + \lambda c_J\right) dR - \sum_{l=1}^{n} \int_R N_l N_J c_J \eta N_L \frac{d\psi_L}{dt}\, dR + \sum_{l'=1}^{n_w} Q_{l'} c_{l'}^* \qquad (31)$$

which can be expressed in the form

$$\dot{\varepsilon}_M = \sum_{l_*=1}^{n_B} F_{l_*}^{B} - \sum_{l=1}^{n} F_l^{s} + \sum_{l'=1}^{n_w} F_{l'}^{w} \qquad (32)$$

where

$$F_{l_*}^{B} = \int_B N_{l_*}\left(D_{ij}\frac{\partial \hat{c}}{\partial x_j} - V_i \hat{c}\right) n_i \, dB$$

$$F_l^{s} = \int_R \phi S_w \kappa N_l N_J \left(\frac{dc_J}{dt} + \lambda c_J\right) dR + \int_R N_J c_J \left(\eta N_l N_L \frac{d\psi_L}{dt}\right) dR \qquad (33)$$

$$F_{l'}^{w} = Q_{l'} c_{l'}^*$$

and L is another dummy nodal subscript. Except for the boundary material flux terms, all other terms in (32) can be evaluated in a simple manner. In particular, the evaluation of F_l^{s} is straightforward if one writes the column vector $\{F^s\}$ for time level $k + 1$ in the form

$$\{F^s\}_{k+1} = \sum_e \left\{\left([B^*]^e + \frac{[\bar{B}]^e}{\Delta t_k}\right)\{c\}_{k+1} - \frac{[\bar{B}]^e}{\Delta t_k}\{c\}_k\right\} + \sum_e \frac{[B]^e}{\Delta t_k}(\{\psi\}_{k+1} - \{\psi\}_k)\{c\}_{k+1} \qquad (34)$$

where $[B^*]^e$ and $[\bar{B}]^e$ are the element mass matrices already evaluated by using (20) and (21), $[B]^e$ is the element storage matrix give by the Galerkin approximation of the water flow equation, $\{\psi\}_k^e$ and $\{\psi\}_{k+1}^e$ are column vectors containing nodal values of ψ at time levels k and $k+1$, respectively, and $\{c\}_{k+1}$ is the column vector containing nodal values of c at the current time level $k+1$.

The evaluation of the boundary material flux $F_{I^*}^B$ is more involved and requires further evaluation. In a case involving the third type boundary condition, the total solute material flux is prescribed according to (11), and thus $F_{I^*}^B$ for time level $k+1$ is given explicitly by

$$F_{I^*}^B = \int_B N_{I^*}\, q_c^T\, dB \tag{35}$$

where the time level index is omitted from $F_{I^*}^B$ and q_c^T for the sake of convenience. Hereafter it is understood that all quantities that are time-dependent are written at the current time level $k+1$. Note that the boundary integral is simple to evaluate, particularly if one uses the procedure described in the first paper. In a case involving the second type boundary condition, the dispersive solute flux is prescribed according to (10), and the advective solute flux is given by

$$-V_i n_i \hat{c} = V_n N_J c_J \tag{36}$$

where V_n is the component of Darcy velocity normal to boundary and is considered positive in the inward direction.

It follows that the term $F_{I^*}^B$ may be expressed as

$$F_{I^*}^B = \int_B N_{I^*}(V_n N_J c_J + q_c^D)\, dB \tag{37}$$

which may be approximated by

$$F_{I^*}^B \simeq c_{I^*} \int_B N_{I^*}\, V_n\, dB + \int_B N_{I^*}\, q_c^D\, dB \tag{38}$$

where the summation convention is not applied to subscript I^*.

Although the boundary integrals in (38) are simple to evaluate, caution should be exercised in dealing with the integral containing the normal component of Darcy velocity V_n. This integral corresponds to the nodal fluid flux for boundary node I^*. It should be evaluated a priori in the previous Galerkin finite element solution of the associated fluid flow problem [*Huyakorn et al.*, 1984]. The nodal fluid flux evaluation should be performed by back substitution of the computed pressure head ψ into the Galerkin finite element equation for node I^*. This procedure avoids the problem of discontinuities in the velocity field and hence discontinuities of the normal velocity V_n at the boundary nodes. Such discontinuities arise if one employs Darcy's equation to compute velocities at the boundary nodes of individual elements and uses these velocities to obtain V_n. The substitution of such values of V_n in (38) usually leads to an incorrect estimate of $F_{I^*}^B$ and, consequently, an incorrect assessment of the mass balance error.

In a case involving the first type or prescribed concentration boundary condition, the dispersive boundary nodal flux of time level $k+1$ is not known explicitly and should also be computed by backsubstitution of c into the original finite element approximation of the transport equation at node I^* (equation (17) with $I = I^*$ and $\omega = 1$). Once the dispersive nodal flux $Q_{cI^*}^D$ has been computed for time level $k+1$, the total boundary nodal flux can be determined from

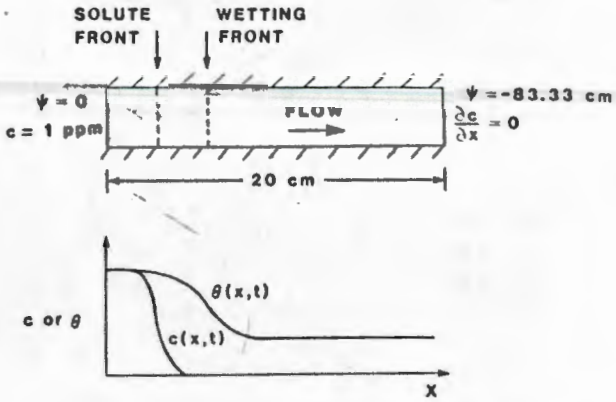

Fig. 2. One-dimensional solute transport during adsorption of water in a soil tube.

$$F_{I^*}^B \simeq c_{I^*} \int_B N_{I^*}\, V_n\, dB + Q_{cI^*}^D \tag{39}$$

After all the various material flux terms have been evaluated the error in the rate of material balance ε_M can be determined from (32). For a general assessment of the accuracy of the numerical solution, a normalized form of ε_M is also presented in the form

$$\|\varepsilon_M\| = \varepsilon_M \Big/ \left[\sum_{I^*=1}^{n_B} |F_{I^*}^B| + \sum_{I=1}^{n} |F_I^s| + \sum_{I'=1}^{n_w} |F_{I'}^w| \right] \tag{40}$$

It should be noted that in practice, the denominator of (40) is usually nonzero, but each of its individual summations may be zero. For example, in a case involving transient flow and transport, the first summation will be zero if there is no solute flux across the entire boundary. In a case involving steady state fluid flow and steady state conservative transport processes, the second summation will be zero. Finally, in a case where there is no internal sources or sinks, the third summation is zero.

ILLUSTRATIVE EXAMPLES

The numerical techniques described in this paper have been incorporated into the SATURN computer code referred to in the first paper [*Huyakorn et al.*, 1984]. Three examples are provided in this section. The examples are chosen for the following purposes: (1) to test and assess the computational efficiency of the given mass balance evaluation scheme under different physical conditions and a variety of boundary conditions, and (2) to demonstrate the utility and accuracy of the present transport model and illustrate certain advantages of the finite element formulation described. In all three examples, it is assumed in the calculation of mass balance that the width normal to the plane of flow is one unit.

Example 1: One-Dimensional Solute Transport During Adsorption of Water in a Soil Tube

This problem is depicted schematically in Figure 2. A conservative solute species is injected into a tube of unsaturated soil that has a uniform initial concentration and moisture content. The initial concentration is assumed to be zero, and the inlet concentration c_0 is assumed to be 1 ppm (mg/L). The solute is transported by dispersion and advection. For the sake of convenience, all physical data pertaining to the geome-

TABLE 1. Value of Physical Parameters Used in Example 1

Parameter	Assigned Value	Units
K	1	cm/d
ϕ	0.45	...
$\psi(x, t = 0)$	−83.33	cm
S_{wr}	0.333	...
ψ_r	−100	cm
ψ_a	0	cm
$c(x, t = 0)$	0	...
τD^*	1	cm²/d
α_L, α_T	0	cm
λ	0	d⁻¹
κ	1	...

Relative permeability versus water saturation: $k_{rw} = (S_w - S_{wr})/(1 - S_{wr})$. Pressure head versus water saturation: $(\psi - \psi_a)/(\psi_r - \psi_a) = (1 - S_w)/(1 - S_{wr})$.

try of the soil tube and the hydraulic properties of the soil material are kept the same as those used in the first paper. The complete set of soil physical data are presented in Table 1. Values of water saturation and Darcy veocity required in the transport simulation were obtained from the finite element simulation of the associated flow problem described in the first paper.

The stated transport problem was solved using a rectangular grid consisting of 35 elements and 72 nodes. The nodal spacings selected are as follows: $\Delta x = 0.25$ for $0 \le x \le 5$, and $\Delta x = 1$ for $5 \le x \le 20$ cm. Time step values were chosen to be $\Delta t = 0.0025$ days. The Crank-Nicolson central difference time stepping was used in conjunction with a small amount of upstream weighting (upstream factor α set equal to 0.1) to control numerical oscillations. Concentration distributions obtained are compared in Figure 3 with the semianalytical result computed using the similarity solution technique described by *Smiles et al.* [1978] and *Watson and Jones* [1982]. Also included in the comparison is the numerical result obtained using the FEMWASTE finite element transport code documented by *Yeh and Ward* [1981]. It can be seen that, in general, both finite element solutions agree reasonably well with the semianalytical solution. As expected, the accuracy of the finite element results is not good at the early time value, $t = 0.01$ day, because the selected values of spatial and time increments are too large to produce accurate approximation of such an early concentration distribution. At later time values the two sets of numerical results agree better with the semianalytical solution. It should be noted, however, that the Galerkin solution produced by FEMWASTE exhibits a rather severe oscillation (overshoot) at the early time value. This os-

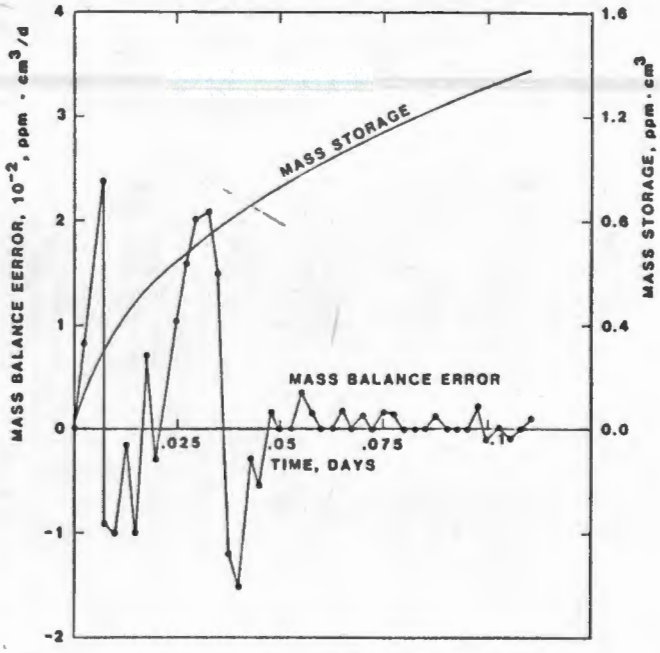

Fig. 4. Cumulative mass storage and mass balance error versus time for example 1.

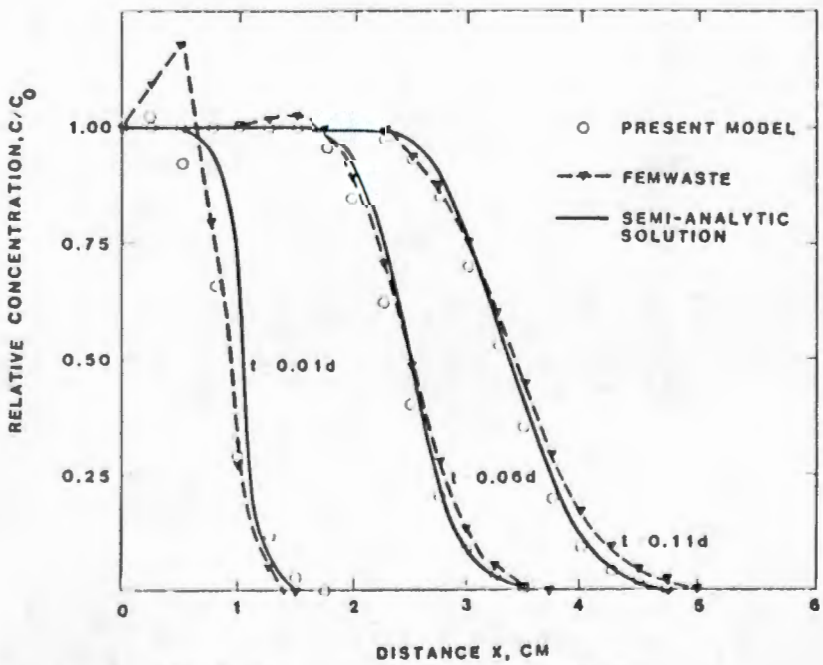

Fig. 3. Computed solute concentration distributions.

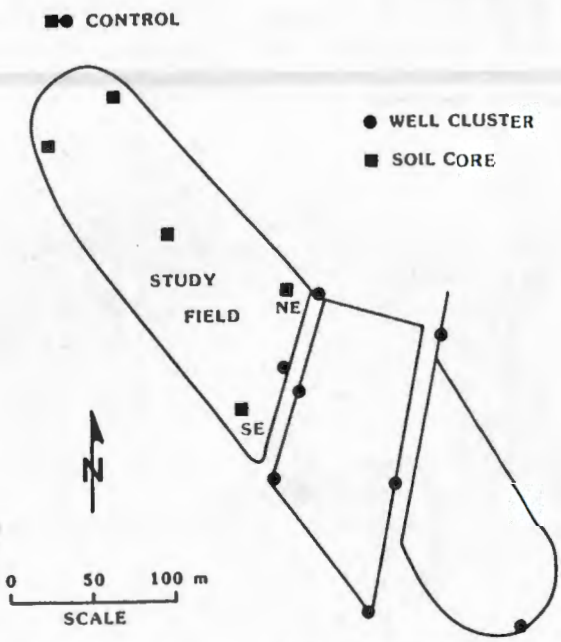

Fig. 5. Test site for aldicarb field study near Cutchogue, New York, showing location for soil sampling and groundwater observation wells.

cillation is quickly dampened at later times leading to concentration fronts that are more smeared than those of the semianalytical solution and the upstream-weighted solution computed by the SATURN code. An explanation for a likely cause of the oscillation problem with FEMWASTE is delayed until we deal with example 3. It may also be noted that the increased nodal spacing beyond the front location did not significantly affect the accuracy of the numerical results shown in Figure 3.

For demonstrative purposes we also provide the mass balance information obtained using the scheme described earlier. Figure 4 illustrates the plot of time versus cumulative storage of solute mass in the soil and time versus mass balance error defined as the difference between the total (advective and dispersive) mass inflow rate and the rate of mass accumulation. The mass storage curve behaves in the manner expected. The mass balance error curve exhibits fluctuations. However, the amplitude of the fluctuations decreases rapidly with time. This is to be expected because the numerical solutions of both the unsaturated flow and the related transport problems were obtained using Picard iteration and Crank-Nicolson schemes that are temporally stable. It should be noted that if, for stance, explicit time stepping schemes were used and the numerical solutions were temporally unstable, the mass balance error would grow with time and eventually its magnitude would become unbounded.

Example 2: One-Dimensional Transport During Infiltration in an Unsaturated Soil System

In this problem, the movement of Temik aldicarb pesticide is considered. Aldicarb, or 2-methyl-2-(methylthio) propionaldehyde 0-(methylcarbamoyl) oxime, is manufactured by the Union Carbide Company and is commonly used to control nematodes. Use of aldicarb in permeable sandy soils provides increased opportunity for leaching of toxic chemicals through soil to groundwater. This has been observed and studied on Long Island, New York [*Enfield et al.*, 1982], and

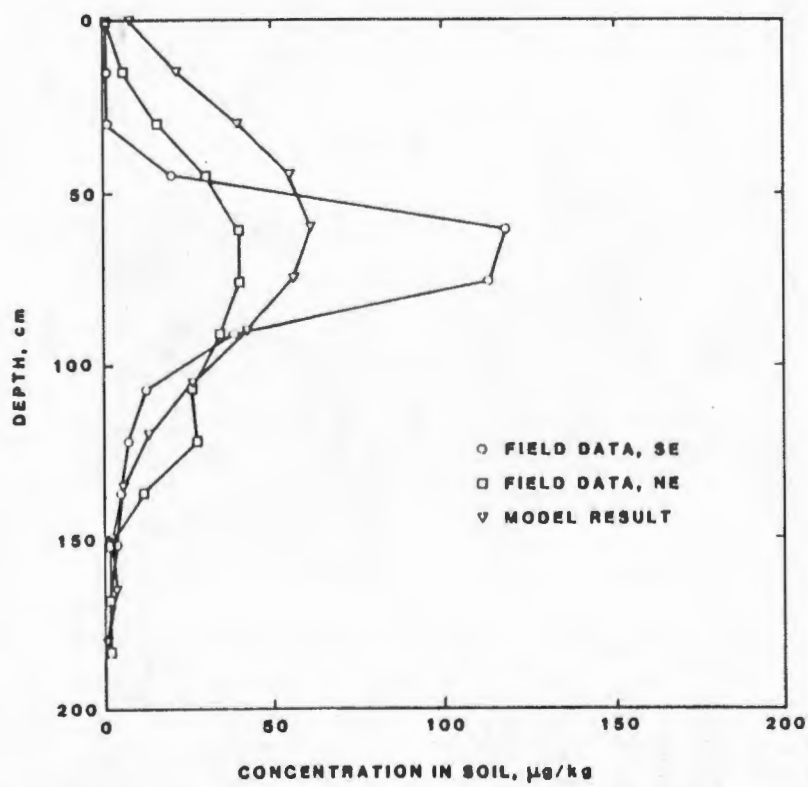

Fig. 6. Comparison of model results and field data for the transport of aldicarb at the site in Cutchogue, New York.

TABLE 2. Value of Physical Parameters Used in Example 2

Parameter	Assigned Value	Units
ϕ	0.38	...
S_w	0.632	...
V	0.0816	cm/d
τD^*	1.44	cm^2/d
α_L, α_T	0	cm
λ	0.00264	d^{-1}
κ	1.456	...
k_d	0.073	cm^3/g
ρ_s	1.5	g/cm^3
c_0	5546	$\mu g/L$
s_0	404.91	$\mu g/kg$

in citrus fields in Florida [*Hornsby et al.*, 1983; *Jones et al.*, 1983].

A field study of aldicarb transport was conducted at a farm located approximately 18 mi (29 km) northeast of Riverhead in eastern Long Island at Cutchogue, New York. The study site is shown in Figure 5 and is approximately 7 acres (2.8 ha) in size.

During December 1979, soil samples were taken at six locations using a bucket auger. Some of the results of this sampling are shown in Figure 6 for the samples taken at the northeast (NE) and southeast (SE) corners of the study field.

Data for the case simulated by the present model are given in Table 2. These were determined from the information provided by *Enfield et al.* [1982], where we have corrected his velocity [*Enfield et al.*, 1982, p. 719]. Only the 1979 application of aldicarb to the field is considered here. The simulation was performed over a depth of 240 cm using a vertical grid consisting of 34 nodes and 16 elements. The nodal spacings were $\Delta x = 15$ cm and $\Delta z = 15$ cm starting at the surface and extending to the water table at the depth of 240 cm. The problem was solved using the Galerkin scheme with the central difference temporal approximation. A variable time step was used with an initial time step of 1.08 days, a multiplier of 1.2, and a maximum time step of 5 days. Relative concentration values were computed, where the zero value corresponds to uncontaminated water and the unit value corresponds to water that contains aldicarb in its application concentration c_0.

Recharge at the top was allowed and the injected water was considered to have a relative concentration of zero. Nonuniform initial conditions were used, with the contaminant slug in place at the top. To achieve this, the initial concentration was set equal to c_0 for the top element nodes and equal to zero elsewhere. The value of c_0 is given in Table 2 and was computed based on the actual volume of aldicarb applied and the pore volume of the top two grid blocks.

Results from this simulation after 242 days are also plotted on Figure 6, where these are the soil concentrations obtained by multiplying the solute concentration by a factor of $k_d = s_0/c_0$, where s_0 is the initial sorbed concentration of the soil. The values of s_0 and c_0 are given in Table 2. As may be seen, the peak concentrations occur at approximately 60 cm depth.

The results of this simulation compare well with the results from an analytical solution presented by *Enfield et al.* [1982]. These results demonstrate (1) persistence ($\lambda = 0.00264$ d^{-1}), (2) mobility ($V = 0.0816$ cm/d and $k = 1.456$), and (3) short distance to the water table ($z = 240$ cm).

Mass balance information is presented in Figure 7. Only the mass decay curve is shown because the mass storage curve is the same shape but opposite in sign. Also depicted in the same figure is the mass balance error as a function of time. Once again the magnitude of the error decreases rapidly with time. However, the error in this example behaves differently from

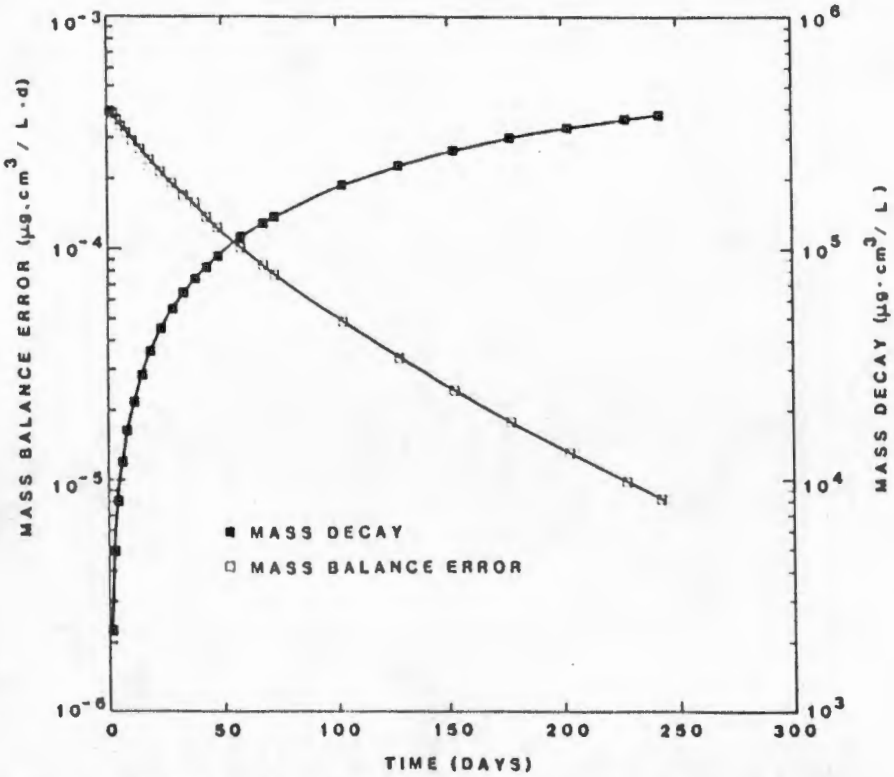

Fig. 7. Computed relations of mass decay and mass balance error versus time for example 2.

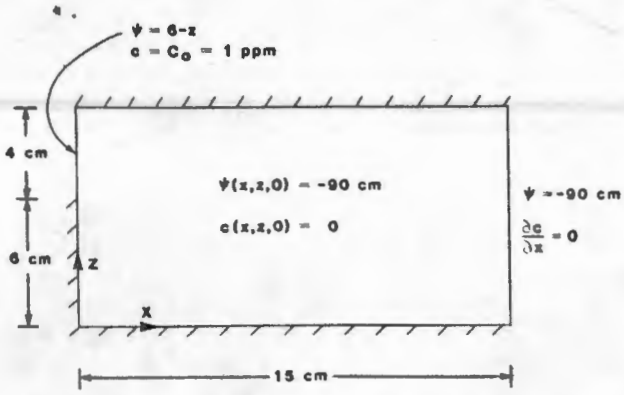

Fig. 8. Two-dimensional transport in an unsaturated soil slab.

example 1. In the present case, there is no fluctuation with time. Furthermore, the magnitude of the observed error is much smaller than that for example 1. A possible explanation for this is the fact that in this example a uniform steady state velocity distribution was used in solving the transport equation (7). Such a velocity field satisfies the continuity equation (5) for flow exactly. Consequently, the computed concentration satisfies the mass balance criterion much better than in example 1, where inexact transient velocity and water saturation distributions were used to obtain the numerical solution.

Example 3: Two-Dimensional Transport in an Unsaturated Soil Slab

This problem concerns transport of a nonconservative solute in a rectangular cross section of an unsaturated soil. As illustrated in Figure 8, the soil is initially dry and water and solute are allowed to enter the system at the upper portion of the left-hand boundary, $x = 0$ and $6 \leq z \leq 10$ cm. The right-hand boundary, which corresponds to the outlet, is maintained at the same initial pressure head value. At the inlet, the pressure head is maintained at $\psi = 6 - z$, and the solute concentration is assumed to be 1 ppm. No flow and zero normal concentration gradients are applied to the remaining portions of the entire boundary.

Values of the physical parameters required are given in Table 3. Once again, values of water saturation and Darcy velocities at different times were determined by analyzing the associated flow problem. Both flow and transport were simulated using a medium rectangular grid. The grid was a uniform 11 × 16 grid composed of 176 nodes and 150 elements.

TABLE 3. Values of Physical Parameters Used in Example 3

Parameter	Assigned Value	Units
K	1	cm/d
ϕ	0.45	...
$\psi(x, z, 0)$	-90	cm
S_{wr}	0.333	...
ψ_r	−100	cm
ψ_a	0	cm
$c(x, z, 0)$	0	...
x_L	1	cm
x_r	0	cm
τD^*	0.01	cm²/d
λ	0.001	d⁻¹
κ	2	...

Soil moisture relations are given in Table 1.

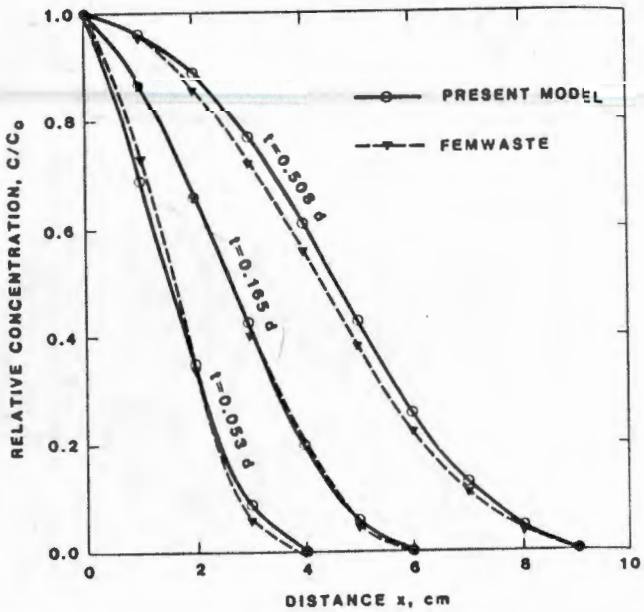

Fig. 9. Computed horizontal distributions of solute concentration at $z = 10$ cm.

The nodal spacings were $\Delta x = \Delta z = 1$ cm. Time increment values were generated within the code using the algorithm: $\Delta t_1 = 0.01$ days, $\Delta t_k = 1.2\,\Delta t_{k-1} \leq 0.05$ day.

The transport simulation was performed for 15 time steps using the Galerkin scheme. (Upstream weighting was not applied in this case because the cell Peclet number, $Pe = \Delta x/\alpha_L$, was not large enough to create numerical difficulties). For verification purposes, the solution obtained using the present finite element model is compared in Figures 9 and 10 with the corresponding Galerkin solution obtained using the FEMWASTE code. Evidently, the overall agreement between the two numerical solutions is reasonable. The horizontal concentration distributions depicted in Figure 9 are all smooth,

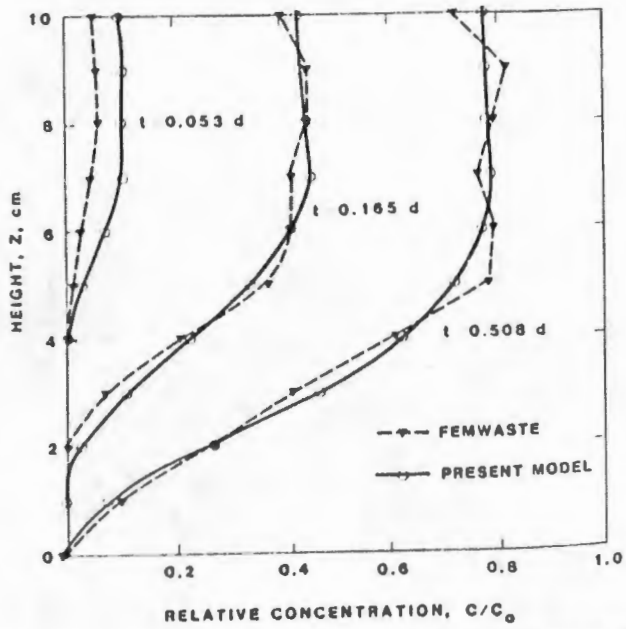

Fig. 10. Computed vertical distributions of solute concentration at $x = 3$ cm.

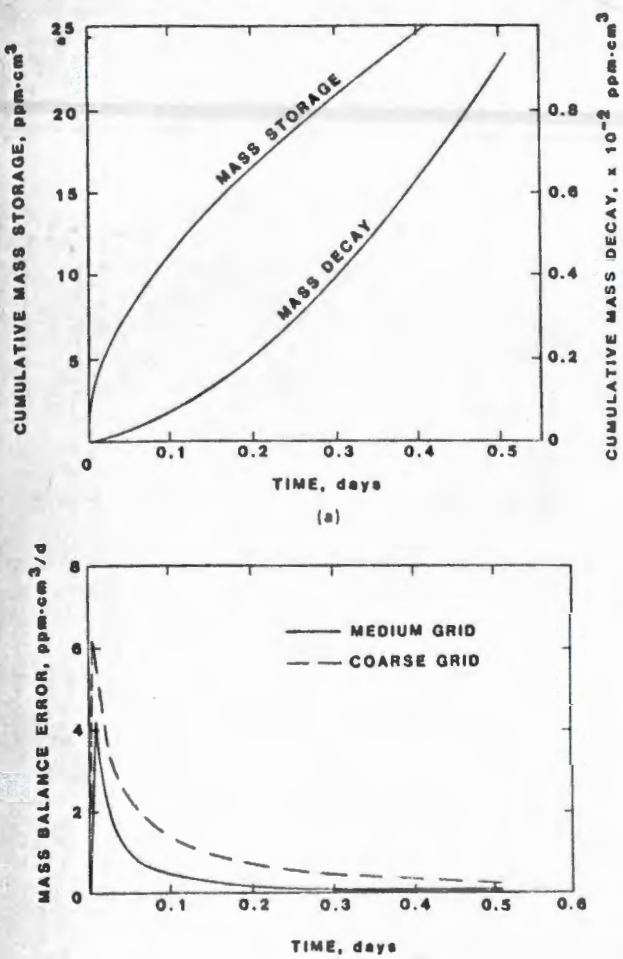

Fig. 11. Mass storage, mass decay, and mass balance error curves for example 3.

although the profile predicted by the present model appears to be slightly ahead of that predicted by FEMWASTE. Note, however, that at the two later time values the vertical concentration distributions computed by FEMWASTE exhibit undesirable oscillations and incorrect representation of the zero normal gradient boundary condition at the top boundary, $z = 10$ cm. In contrast, the vertical concentration profiles computed by the present model are smooth. Furthermore, the zero normal gradient condition at $z = 10$ cm is very well duplicated.

We believe that the numerical oscillation problem experienced by FEMWASTE is associated with the manner in which the Galerkin approximation of the transport equation is performed. As described by *Duguid and Reeves* [1976] and *Yeh and Ward* [1981], the finite element formulation employed in FEMWASTE is achieved by applying Green's theorem to both the dispersive and the advective terms of the primitive transport equation. Such a formulation provides a convenient way to accommodate third-type material flux boundary conditions. Unfortunately, it is highly sensitive to errors in the computation of Darcy velocity and fluid flux values [see *Huyakorn and Pinder*, 1983, p. 199]. In other words, small errors in the estimate of the fluxes can trigger sizable oscillations of concentration values adjacent to the flow boundary. Experience indicates that these oscillations may be dampened as time goes on or they may persist throughout the remaining simulation time period.

Unlike the finite element formulation used in FEMWASTE, the present formulation is achieved by using the transformed version of the transport equation (see equation (7)) and applying Green's theorem only to the dispersive term. This leads to the numerical scheme that is much less oscillation prone. In addition, the mass balance computational algorithm also works well in two dimensions. This is evident in the result presented in Figure 11. In Figure 11*a*, the behavior of the mass storage and decay curves may be noted. In Figure 11*b*, it is seen that the mass balance error for the problem solved behaves in a similar manner to that in example 2. Of particular interest is the fact that the mass balance error corresponding to the medium grid with 176 nodes is substantially less than that corresponding to a coarser grid consisting of 96 nodes. The reason for this is the manner in which the finite element solution and the mass balance schemes are formulated. It may be recalled that the mass balance criterion used is an integral representation of the original transport equation (3). On the other hand, the numerical solution is formulated using the converted transport equation (7), which is equivalent to the original transport equation (3), provided the continuity equation for water flow (5) is satisfied. If the velocity field and the water saturation distribution used in the transport analysis do not satisfy the continuity equation for flow, a significant mass balance error will be detected when the computed concentration is substituted into the solute mass balance integral equation.

As depicted in Figure 11, the mass balance error is greater with the coarse grid than with the medium grid because the velocity field and water saturation distribution computed using the coarse grid are less accurate than those computed using the medium grid. It is also interesting to note that the mass balance error from the analysis of two-dimensional flow and transport is considerably less than that from the one-dimensional analysis. This may be seen by comparing Figure 11 with Figures 4 and 7.

DISCUSSION AND CONCLUSIONS

One major point that remains to be discussed is the computational efficiency of the numerical techniques presented. We first consider the influence coefficient technique for element matrix evaluation. Implementation of this technique into the SATURN code has led to substantial saving of the CPU time. In a general case where upstream weighting is used, the CPU cost of the influence coefficient procedure is no more than 8% of the Gauss quadrature integration procedure used in the previous papers by *Huyakorn and Nilkuha* [1979] and *Yeh and Ward* [1982].

In addition to the influence coefficient technique for element matrix evaluation, the mass balance computational scheme presented in this paper is also cost effective. Table 4 provides the CPU seconds required by the SATURN code to run each of the three example problems on the PRIME 550/model II minicomputer. The CPU cost for a 15 time step run of problem 3 using the finest mesh (341 nodes) is approximately $6.00 with the mass balance option and $5.40 without the mass balance option. As illustrated in Table 4, the mass balance computational scheme requires between 10 and 30% of the total CPU time depending on the number of nodes in the finite element mesh: the larger the number of nodes used, the smaller is the percentage CPU time required by the mass balance scheme. The relationship between the percentage difference in CPU time and the number of nodal points is plot-

TABLE 4. CPU Seconds Taken by PRIME 550 (Model II) Minicomputer

Problem	Number of Nodes	Number of Time Steps	CPU Seconds		Percentage Difference
			Mass Balance	No Mass Balance	
1	72	44	80.39	59.84	25.6
2	34	55	32.64	22.80	30.2
3	96	15	51.43	38.73	24.7
3	176	15	108.64	88.73	24.7
3	341	15	304.2	269.94	11.3

ted in Figure 12 on a semilogarithmic scale. Evidently, this relationship is well fitted by a straight line within the range of the number of nodes considered.

The mass balance scheme presented in this paper is considerably more efficient than that presented earlier by *Yeh* [1981]. This is because the latter involves the determination of nodal values of Darcy velocity components by solving a set of $2n$ simultaneous equations. For cases involving transient variably saturated flow and transport, such a solution must be performed for each time step and is rather costly. Each nodal velocity solution would require at least 8 times the CPU time required in solving for nodal concentration values simply because both the number of algebraic equations, n, and the matrix bandwidth, B, are doubled and the solution time is proportional to nB^2.

On the other hand, the present mass balance scheme does not involve such a tedious Darcy velocity computation. Instead, boundary fluid and solute fluxes are determined by backsubstitution of the nodal head and concentration values into specific rows of the global matrix equations already derived in the solution process. The rows that need to be considered would be those corresponding to the boundary nodes where nonzero fluxes occur.

In closing, we would like to indicate that our mass balance scheme is one of several mass balance schemes that can be formulated for solute transport in porous media. It should be regarded as just a screening device for examining the numerical solution. One must recognize, however, that a mass balance check provides a necessary but not sufficient condition for ensuring accurate numerical solutions of the governing equations for flow and transport. It is not uncommon to encounter a case where an excellent mass balance check is obtained, and yet the numerical solution of the transport equation displays severe numerical dispersion or oscillations and is grossly inaccurate. An example of such a case is that of transient one-dimensional transport in steady uniform flow in a semi-infinite soil column.

Despite its mentioned drawback, mass balance computation is still useful from a practical standpoint. The usefulness of a reliable mass balance scheme lies in the fact that it allows us to identify unacceptable numerical results that should be viewed with great suspect or discarded because of poor mass balance errors.

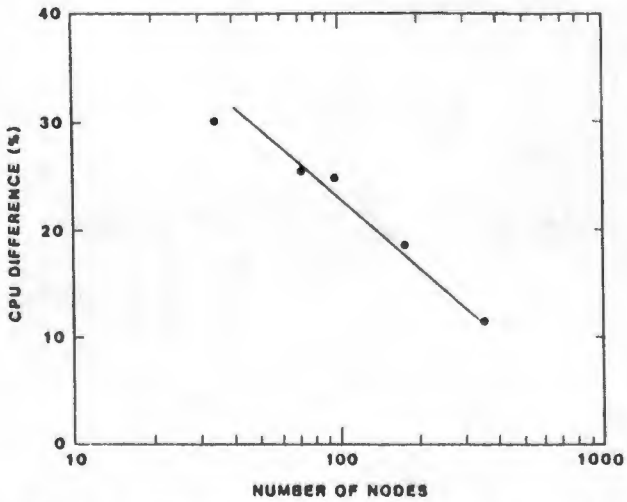

Fig. 12. Number of nodes versus CPU seconds required by SATURN on PRIME 550 minicomputer to solve the given transport problems.

APPENDIX: 1. INFLUENCE COEFFICIENT MATRICES $[E_D^{xx}]^e$, $[E_D^{yy}]^e$, $[E_D^{xy}]^e$, AND $[M]^e$

$$[E_D^{xx}]^e = \frac{1}{6}\begin{bmatrix} 2 & -2 & -1 & 1 \\ -2 & 2 & 1 & -1 \\ -1 & 1 & 2 & -2 \\ 1 & -1 & -2 & 2 \end{bmatrix}$$

$$[E_D^{yy}]^e = \frac{1}{6}\begin{bmatrix} 2 & 1 & -1 & -2 \\ 1 & 2 & -2 & -1 \\ -1 & -2 & 2 & 1 \\ -2 & -1 & 1 & 2 \end{bmatrix}$$

$$[E_D^{xy}]^e = \frac{1}{2}\begin{bmatrix} 1 & 0 & -1 & 0 \\ 0 & -1 & 0 & 1 \\ -1 & 0 & 1 & 0 \\ 0 & 1 & 0 & -1 \end{bmatrix}$$

$$[M]^e = \frac{1}{9}\begin{bmatrix} 4 & 2 & 1 & 2 \\ 2 & 4 & 2 & 1 \\ 1 & 2 & 4 & 2 \\ 2 & 1 & 2 & 4 \end{bmatrix}$$

APPENDIX: 2. INFLUENCE COEFFICIENT MATRICES $[E_v^x]^e$, $[E_v^y]^e$, $[E_v^x]_u^e$, AND $[E_v^y]_u^e$

$$[E_v^x]^e = \frac{1}{6}\begin{bmatrix} -2 & 2 & 1 & -1 \\ -2 & 2 & 1 & -1 \\ -1 & 1 & 2 & -2 \\ -1 & 1 & 2 & -2 \end{bmatrix}$$

$$[E_v^y]^e = \frac{1}{6}\begin{bmatrix} -2 & -1 & 1 & 2 \\ -1 & -2 & 2 & 1 \\ -1 & -2 & 2 & 1 \\ -2 & -1 & 1 & 2 \end{bmatrix}$$

$$[E_v^x]_u^e = \frac{1}{6}\begin{bmatrix} 2\alpha_1 & -2\alpha_1 & -\alpha_1 & \alpha_1 \\ -2\alpha_1 & 2\alpha_1 & \alpha_1 & -\alpha_1 \\ -\alpha_2 & \alpha_2 & 2\alpha_2 & -2\alpha_2 \\ \alpha_2 & -\alpha_2 & -2\alpha_2 & 2\alpha_2 \end{bmatrix}$$

$$[E_v^y]_{ij}^e = \frac{1}{6}\begin{bmatrix} 2\beta_2 & \beta_2 & -\beta_2 & -2\beta_2 \\ \beta_1 & 2\beta_1 & -2\beta_1 & -\beta_1 \\ -\beta_1 & -2\beta_1 & 2\beta_1 & \beta_1 \\ -2\beta_2 & -\beta_2 & \beta_2 & 2\beta_2 \end{bmatrix}$$

NOTATION

B solution boundary.
B_1 prescribed concentration boundary.
B_2 prescribed dispersive flux boundary.
B_3 prescribed total (dispersive and convective) flux boundary.
B^e element boundary.
B_{IJ}^{*e} element matrix associated with decay term.
$\bar{B}_{IJ}^e$ element matrix associated with time derivative.
c concentration of the dissolved constituent, $M\ L^{-3}$.
$\bar{c}$ prescribed boundary concentration, $M\ L^{-3}$.
c_0 initial concentration of dissolved constituent, $M\ L^{-3}$.
c_s concentration of adsorbed constituent in the solid phase, $M\ L^{-3}$.
c^* concentration of the constituent in the injected fluid, $M\ L^{-3}$.
$\tilde{D}_{ij}$ hydrodynamic dispersion tensor, $L^2\ T^{-1}$.
D_{ij} dispersion coefficient defined in equation (4*a*), $L^2\ T^{-1}$.
D^* coefficient of molecular diffusion, $L^2\ T^{-1}$.
E_{IJ}^e element matrix associated with spatial derivatives.
$[E_D]^e$ element matrix associated with dispersive term.
$[E_v]^e$ element matrix associated with advective term.
F_I^e element right-hand side vector.
i, j coordinate subscripts.
I, J, L nodal subscripts.
k time level index.
k_d distribution coefficient, $L^3\ M^{-1}$.
l, m dimensions of rectangular element, L.
$[M]^e$ influence coefficient mass matrix.
n number of nodes in the finite element network.
n_i outward unit normal vector.
n_B number of nodes on the boundary.
n_w number of wells.
N_I, N_J basis functions.
q volumetric flow rate per unit volume of the medium, T^{-1}.
q_c^D prescribed boundary dispersive flux, $M\ L^{-2}\ T^{-1}$.
q_c^T prescribed boundary total flux, $M\ L^{-2}\ T^{-1}$.
$Q_{I\prime}$ volumetric rate of well at node I, $L^3\ T^{-1}$.
R solution domain.
R^e element subdomain.
S_s specific storage, L^{-1}.
S_w water saturation.
s_0 initial sorbed concentration on the soil.
t elapsed time, T.
V_i flow velocity in the x_i direction, $L\ T^{-1}$.
V_n Darcy flux at the boundary, $L\ T^{-1}$.
W_I weighting function for node I.
x_i component of the Cartesian coordinate system, L.
α_L longitudinal dispersivity, L.
α_T transverse dispersivity, L.
δ_{ij} Kronecker delta.
$\dot{\varepsilon}_M$ rate of material loss, $M\ T^{-1}$.
κ retardation coefficient defined in equation (4*b*).
λ decay constant, T^{-1}.
η overall storate coefficient L^{-1}.
τ tortuosity.
ω time weighting factor.
ϕ porosity.
ρ_B bulk density, $M\ L^{-3}$.
ρ_s density of the solid material, $M\ L^{-3}$.
ψ pressure head, L.

Acknowledgments. This work was supported, in part, by research funds provided by GeoTrans, Inc. Additional funding was made possible by EPRI Technical Services Agreement RP1619-2 between GeoTrans, Inc. and the Electric Power Research Institute. The authors wish to acknowledge Ishwar P. Murarka (EPRI) and Atef Elzeftawy (U.S. Nuclear Regulatory Commission) for their help and encouragement.

REFERENCES

Bear, J., *Hydraulics of Ground Water*, 569 pp., McGraw-Hill, New York, 1979.

Bresler, E., Simultaneous transport of solutes and water under transient unsaturated flow conditions, *Water Resour. Res.*, *9*, 975–986, 1973.

Bresler, E., and R. J. Hanks, Numerical method for estimating simultaneous flow of water and salt in unsaturated soils, *Soil Sci. Soc. Am. Proc.*, *33*, 827–832, 1969.

Duguid, J., and M. Reeves, Material transport in porous media: A finite element Galerkin model, *Rep. ORNL-4928*, Oak Ridge Natl. Lab., Oak Ridge, Tenn., 1976.

Enfield, C. G., R. F. Carsel, S. Z. Cohen, T. Phan, and D. M. Walters, Approximating pollutant transport to groundwater, *Ground Water*, *20*, 711–722, 1982.

Gresho, P. M., R. L. Lee, and R. L. Sani, Advection-dominated flows, with emphasis on the consequences of mass lumping, in *Proceedings of the Second International Symposium on Finite Element Methods in Flow Problems*, edited by S. Margherita, pp. 745–756, International Centre for Computer Aided Design, Ligure, Italy, 1976.

Hornsby, A. G., P. S. C. Rao, P. Nkedi-Kizza, W. B. Wheeler, and R. B. Jones, Fate of aldicarb in Florida citrus soils, 1, Field and laboratory studies, paper presented at the Conference on Characterization and Monitoring of the Vadose (Unsaturated) Zone, Natl. Water Well Assoc. and U.S. Environ. Prot. Agency, Las Vegas, Nev., Dec. 8–10, 1983.

Huyakorn, P. S., Solution of steady-state, convective transport equation using an upwind finite element scheme, *Appl. Math. Modelling*, *1*, 187–195, 1977.

Huyakorn, P. S., and K. Nilkuha, Solution of transient transport equation using an upstream finite element scheme, *Appl. Math. Modelling*, *3*, 7–17, 1979.

Huyakorn, P. S., and G. F. Pinder, *Computational Methods in Subsurface Flow*, 474 pp., Academic, Orlando, Fla., 1983.

Huyakorn, P. S., S. D. Thomas, and B. M. Thompson, Techniques for making finite elements competitive in modeling flow in variably saturated porous media, *Water Resour. Res.*, *20*, 1099–1115, 1984.

Jones, R. B., P. S. C. Rao, and A. G. Hornsby, Fate of aldicarb in Florida citrus soils, 2, Model evaluation, paper presented at the Conference on Characterization and Monitoring of the Vadose (Unsaturated Zone), NWWA and U.S. Environ. Prot. Agency, Las Vegas, Nev., Dec. 8–10, 1983.

Kirda, C., D. R. Nielsen, and J. W. Biggar, Simultaneous transport of chloride and water during infiltration, *Soil Sci. Soc. Am. Proc.*, *37*, 339–345, 1973.

Mercer, J. W., P. S. C. Rao, and I. W. Marine, *Role of the Unsaturated Zone in Radioactive and Hazardous Waste Disposal*, 339 pp., Ann Arbor Science, Ann Arbor, Mich., 1983.

Oster, C. A., Review of ground-water flow and transport models in the unsaturated zone, *Rep. NUREG/CR-2917*, U.S. Nucl. Regul. Comm., Washington, D. C., 1982.

Pickens, J. F., and R. W. Gillham, Finite element analysis of solute transport under hysteretic unsaturated flow conditions, *Water Resour. Res.*, *16*, 1071–1078, 1980.

Segol, G., A three-dimensional Galerkin finite element model for the analysis of contaminant transport in saturated-unsaturated porous media, in *Proceedings, 1st International Conference on Finite Elements in Water Resources*, edited by W. G. Gray, G. F. Pinder, and C. A. Brebbia, pp. 2.123–2.144, Pentech, London, 1977.

Smiles, D. E., J. R. Philip, J. H. Knight, and D. E. Elrick, Hy-

drodynamic dispersion during absorption of water by soil, *Soil Sci. Soc. Am. J.*, *42*, 229–234, 1978.

van Genuchten, M. T., and W. J. Alves, Analytical solutions of the one-dimensional convective-dispersive solute transport equation, *Tech. Bull. 1661*, 151 pp., U.S. Dep. of Agric., Riverside, Calif., 1982.

van Genuchten, M. T., G. F. Pinder, and W. P. Saukin, Modeling of leachate and soil interactions in an aquifer, Management of Gas and Leachate in Landfills, *Rep. EPA-600/9-77-026*, pp. 95–103, U.S. Environ. Prot. Agency, Cincinnati, Ohio, 1977.

Warrick, A. W., J. W. Biggar, and D. R. Nielsen, Simultaneous solute and water transfer in an unsaturated soil, *Water Resour. Res.*, *7*, 1216–1225, 1971.

Watson, K. K., and M. J. Jones, Hydrodynamic dispersion during absorption in a fine sand, 1, The constant concentration case, *Water Resour. Res.*, *18*, 91–100, 1982.

Yeh, G. T., On the computation of Darcian velocity and mass balance in the finite element modeling of ground water flow, *Water Resour. Res.*, *17*, 1529–1534, 1981.

Yeh, G. T., and D. S. Ward, FEMWASTE: A finite-element model of waste transport through saturated-unsaturated porous media, *Rep. ORNL-5601*, 137 pp., Oak Ridge Natl. Lab., Oak Ridge, Tenn., 1981.

P. S. Huyakorn, J. W. Mercer, and D. S. Ward, GeoTrans, Inc., 209 Elden Street, Suite 301, Herndon, VA 22070.

(Received June 18, 1984;
revised November 13, 1984;
accepted November 29, 1984.)